Journal of Solid State Chemistry 182 (2009) 2443–2450

Contents lists available at ScienceDirect

Journal of Solid State Chemistry

journal homepage: www.elsevier.com/locate/jssc

Synthesis, crystal structure, spectroscopic and thermal properties of $[Et_4N][Ta_6Br_{12}(H_2O)_6]Br_4 \cdot 4H_2O$ (Et = ethyl)—A new compound with the paramagnetic $[Ta_6Br_{12}]^{3+}$ cluster core

Berislav Perić [a,**], Dražan Jozić [a,1], Pavica Planinić [a,*], Nevenka Brničević [a], Gerald Giester [b]

[a] Ruđer Bošković Institute, Bijenička cesta 54, 10000 Zagreb, Croatia
[b] Institut für Mineralogie und Kristallographie, Universität Wien–Geozentrum Althanstraße, 14, 1090 Wien, Austria

ARTICLE INFO

Article history:
Received 4 March 2009
Received in revised form
5 June 2009
Accepted 17 June 2009
Available online 24 June 2009

Keywords:
Tantalum
Bromide
Hexanuclear cluster
Synthesis
Crystal structure
Paramagnetic cluster

ABSTRACT

A new hexanuclear cluster compound, $[Et_4N][Ta_6Br_{12}(H_2O)_6]Br_4 \cdot 4H_2O$ (Et = ethyl) (**1**), with the paramagnetic $[Ta_6Br_{12}]^{3+}$ cluster entity, was synthesized and characterized by elemental and TG/DTA analyses, IR and UV/Vis spectroscopy and by a single-crystal X-ray diffraction study. The presence of the paramagnetic $[Ta_6Br_{12}]^{3+}$ unit was confirmed also by the room-temperature magnetic and EPR measurements. The compound crystallizes in the tetragonal $I4_1/a$ space group, with $a = 14.299(5)$, $c = 21.241(5)$ Å, $Z = 4$, $R_1(F)/wR_2(F^2) = 0.0296/0.0811$. The structure contains discrete $[Ta_6Br_{12}(H_2O)_6]^{3+}$ cations with an octahedron of metal atoms edge-bridged by bromine atoms and with water molecules occupying all six terminal positions. The cluster units are positioned in the vertices of the three-dimensional (pseudo)diamond lattice. The structure shows similarities with literature reported structures of cluster compounds crystallizing in the diamond ($Fd\bar{3}m$) space group.

1. Introduction

The compounds with edge-bridged octahedral cluster units of the general formula $[(M_6X^i_{12})L^a_6]$ [M = Nb, Ta; X^i = inner, bridging ligand (halogen atoms); L^a = apical, terminal ligand (H_2O, OH^-, Cl^-, Br^-, CN^-…)] stand for the most significant part of niobium and tantalum halide cluster chemistry ever since their discovery. The existence of several different oxidation states of the $[M_6X^i_{12}]^{n+}$ cluster unit ($n = 2$, 3, 4) is the main specificity of these compounds. The clusters with $n = 2$ or 4 are diamagnetic, whereas those with $n = 3$ are paramagnetic [1–5]. The molecular orbital model wherein the highest occupied molecular orbital (HOMO) of the $[M_6X^i_{12}]^{n+}$ cluster core is an orbital singlet, doubly occupied when $n = 2$, singly occupied when $n = 3$ and empty (LUMO) when $n = 4$ makes clear the above mentioned behaviour [6]. For a successful study of magneto-structural correlations of paramagnetic clusters detailed structural analyses of the crystal packing features of these compounds should be made. Heretofore, single crystal X-ray diffraction data have been accessible for a number of paramagnetic tantalum and niobium hexanuclear clusters [3–5,7], but their magnetic susceptibility data are rather scarce in the literature. Magnetic exchange interactions between paramagnetic cluster units (intercluster interactions) were detected for $[(Ta_6Cl_{12})Cl(H_2O)_5]CdBr_4 \cdot 6H_2O$ [3], $[(Ta_6Br_{12})Br_3]$ [4] and $Lu[(Nb_6Cl_{12})Cl_6]$ [8]. A temperature dependent measurement of the inverse intensity of an EMR line of the $[Nb_6F_{12}]^{3+}$ cluster unit also confirmed intercluster interactions [5].

Here we report on the synthetic procedure, single crystal X-ray structure determination and spectroscopic properties for a novel compound of the composition $[Et_4N][Ta_6Br_{12}(H_2O)_6]Br_4 \cdot 4H_2O$, containing the paramagnetic $[Ta_6Br_{12}]^{3+}$ entity. In respect of other compounds with the same cluster core, only structural data for $[(Ta_6Br_{12})Br_3]$ are thus far available in the literature [7a], alongside with the unit cell parameters that were reported for a series of clusters of the composition $RETa_6Br_{18}$ (RE = Y and Nd to Tm; space group $R\bar{3}$ [9].

2. Experimental

2.1. Materials and methods

The starting cluster $Ta_6Br_{14} \cdot 8H_2O$ was prepared by a high-temperature solid-state chemical reaction according to the literature data [10]. The $[Ta_6Br_{12}(EtOH)_6]Br_2$ precursor was prepared from the starting cluster with the use of high-vacuum

** Also corresponding author.
* Corresponding author. Fax: +385 1 468 0098.
E-mail addresses: bperic@irb.hr (B. Perić), planinic@irb.hr (P. Planinić).
[1] Present address: Faculty of Chemistry and Technology, University of Split, Teslina 10, 21000 Split, Croatia.

0022-4596/$ - see front matter © 2009 Elsevier Inc. All rights reserved.
doi:10.1016/j.jssc.2009.06.026

line and Schlenk techniques, following the procedure described earlier [11]. Tetraethylammonium bromide, Et_4NBr, was purchased from Aldrich and dried at 105 °C before use. Absolute ethanol (p.a. Kemika) was dried over sodium ethoxide which was prepared by dissolving metallic sodium in ethanol, following distillation on a high-vacuum line onto activated 3 Å molecular sieves.

Magnetic susceptibility measurements were performed at room temperature, with a Gouy balance (Stanton Instruments SM-12), using $CuSO_4 \cdot 5H_2O$ as calibrant. The EPR measurement was performed on a powdered sample of **1** with an X-band EPR spectrometer (Bruker Elexsys 580 FT/CW) that was equipped with a standard Oxford Instruments model DTC2 temperature controller. The measurement was obtained at the microwave frequency around 9.6 GHz with the magnetic field modulation amplitude of 1 mT at 100 kHz. Infrared spectra were recorded by using KBr pellets with an ABB Bomem FT model MB 102 spectrometer, in the 4000–200 cm^{-1} region. Far-infrared spectra, in the 700–100 cm^{-1} region, were recorded by using polyethylene pellets with a Fourier transform-infrared (FT-IR) Perkin-Elmer 2000 spectrometer. Electronic spectra were measured with a Cary 50 probe spectrophotometer. The samples were prepared as KBr pellets which were mounted in the pathway of the radiation beam, and a weighed pure-KBr pellet was used as a reference. Thermal analysis of **1** was performed on a Shimadzu DTG-60H analyzer, with a heating rate of 10 °C min^{-1} in the stream of synthetic air.

The elemental analysis for C, H and N was carried out by using a Perkin-Elmer model 2400 microanalytical analyzer. Tantalum was determined by the "H-tube" method [12] as well as from the amount of Ta_2O_5 remained after the thermal decomposition of the sample during the TG/DTA analysis. The amount of bromine was determined by potentiometric titration with standard $AgNO_3$ solution after decomposition of the cluster with KOH and H_2O_2.

2.2. Synthesis of **1**

A suspension of the $[Ta_6Br_{12}(EtOH)_6]Br_2$ precursor (0.300 g; 0.121 mmol) in dried ethanol (10 ml) distilled from the high-vacuum line in a round-bottom flask was open in the air and a solution of Et_4NBr (0.051 g; 0.242 mmol) in ethanol (10 ml, 96%) was added. The reaction mixture was stirred magnetically until a clear emerald-green solution was reached (~3 h). The clear solution was transferred into a glass beaker and left at ambient conditions to evaporate. A slight amount of single crystals of the title compound might appear during evaporation, but usually the ethanolic solution evaporates to dryness (in a period of ~7 d) giving only an undefined solid. The so-obtained solid was then treated with redistilled water (10 ml), the mixture stirred magnetically for 1 h and left for further 4 h, when a small amount of an undissolved residue was filtered off. The clear filtrate was left at ambient conditions to slowly evaporate (usually for ~2 weeks) until dark-brown octahedra-like single crystals of **1** came out. The crystals were collected, washed with a very small amount of water and shortly dried in air. Yield: 63%. *Anal.* Calc. for $C_8H_{40}NBr_{16}O_{10}Ta_6$: C, 3.59; H, 1.51; N, 0.52; Br, 47.80; Ta, 40.59. Found: C, 3.64; H, 1.50; N, 0.50; Br, 48.32; Ta, 41.07%. IR (KBr, cm^{-1}): 3475 (w), 3405 (m), 3211 (w), 3065 (w, br), 2974 (w), 2921 (w), 2851 (w), 1620 (m, sh), 1608 (s, sp), 1469 (sh), 1449 (m), 1398 (m), 1303 (w), 1182 (m), 1078 (w), 1032 (m), 1004 (m), 840 (w, br), 792 (s), 568 (sh), 543 (m), 499 (m), 384 (w), 230 (s), 226 (s), 202 (w), 177 (m), 171 (m), 150 (m), 133 (w), 124 (w), 119 (m), 104 (w).

2.3. Single-crystal structure determination

A dark-green octahedral crystal of $[Et_4N][Ta_6Br_{12}(H_2O)_6]Br_4 \cdot 4H_2O$ was selected and attached to the top of a glass capillary. The crystal was mounted under a stream of cold nitrogen at 200(3) K on the goniometer head of a Nonius Kappa-CCD diffractometer. The unit cell parameters, obtained from all measured reflections, were refined according to the *I*-centred tetragonal lattice using the DENZO-SCALEPACK program [13]. The data were corrected for absorption by the multi-scan method of the same program [14]. Almost all non-hydrogen atoms were found by direct methods with the SIR92 program [15] (space group $I4_1/a$), except for the carbon atoms from $[Et_4N]^+$ cations which were found from succeeding difference Fourier syntheses calculated with the SHELXL-97 program [16]. Eight peaks around the nitrogen atom indicated two sets of the four expected positions for the methylene carbons of the $[Et_4N]^+$ cation and were interpreted as an orientational disorder of the symmetry independent CH_2 fragment. So, in the subsequent steps of the analysis the occupancies of both orientations were refined, constraining the sum of the individual occupancies to 1. Hydrogen atoms of the ethyl groups were placed in the calculated positions and constrained to ride on the carbon atoms to which they were bonded, taking into account the individual occupancies of the two methylene orientations. The extinction was taken into account by the method used in the SHELXL-97 program [16] [the coefficient obtained is 0.00037(2)]. Due to a fairly low residual electron density achieved it was possible to find out the most probable positions for hydrogen atoms of all water molecules among the highest peaks in the difference Fourier map. In the final least-squares refinements (full matrix on all reflections, F^2 based) the geometries of these water molecules were restrained to the ideal values (O–H distances to 0.84 Å and H–O–H angles to 104°) and their orientations were left unrestrained. The last refinement was performed including the weighting scheme suggested by the SHELXL-97 program [16] and it converged at $R_1(F)/wR_2(F^2) = 0.0296/0.0811$. The low residual electron density and a good refinement convergence confirmed a good quality of the structural data. The details about data collection and refinement are given in Table 1.

Table 1
Selected crystallographic data and refinement parameters for **1**.

Chemical formula	$[Et_4N][Ta_6Br_{12}(H_2O)_6]Br_4 \cdot 4H_2O$
Formula weight (g mol^{-1})	2674.51
Crystal dimensions (mm^3)	0.08 × 0.08 × 0.08
Crystal system	Tetragonal
Space group	$I4_1/a$ (no. 88)
Unit cell parameters	
a (Å)	14.299(5)
c (Å)	21.241(5)
V ($Å^3$)	4343(2)
Z	4
Density, ρ_{calc} (g cm^{-3})	4.090
Temperature (K)	200(3)
Range of data collection (deg)	$5.56 \le 2\theta \le 61$
μ (Mo$K\alpha$, mm^{-1})	29.810
Diffractometer	Enraf-Nonius KappaCCD
Radiation	Mo$K\alpha$ ($\lambda = 0.71073$ Å)
No. of measured reflections	37 007
No. of unique reflections; R_{int}	3313; 0.0819
Variables	120
$R_1(F)$[a]	0.0296
$wR_2(F^2)$[b]	0.0811
Goodness of fit on F^2	1.148
Max./min. peak (e $Å^{-3}$)	+1.388/−1.147

[a] $R_1 = (\Sigma||F_0| - |F_C||)/(\Sigma|F_0|)$ for 2936 reflections with $I_0 > 2\sigma(I_0)$.

[b] $wR_2 = \sqrt{(\Sigma w(|F_0^2| - |F_c^2|)^2)/(\Sigma w(F_0^2)^2)}$ for all data, with $w = 1/[\sigma^2(F_0^2) + (0.0058P)^2 + 45.8484P]$ where $P = [2F_c^2 + \max(F_0^2, 0)]/3$.

3. Results and discussion

3.1. Synthesis and properties

The title compound, $[Et_4N][Ta_6Br_{12}(H_2O)_6]Br_4 \cdot 4H_2O$ **1**, was obtained when ethanolic solutions of the $[Ta_6Br_{12}(EtOH)_6]Br_2$ precursor and of tetraethylammonium bromide, Et_4NBr, taken in the molar ratio of 1:2, were allowed to react at ambient conditions, and the solvent left to evaporate to dryness. The so-obtained solid was then dissolved in water and after a period of ~2 weeks nicely shaped, dark-brown octahedral crystals of **1** emerged. Obviously, during this treatment ethanol molecules from the terminal octahedral coordination sites of the cluster were exchanged by water molecules, followed by a slow oxidation process of $[Ta_6Br_{12}]^{2+}$ to $[Ta_6Br_{12}]^{3+}$ by air-oxygen. Once formed, the compound is almost insoluble in water and only very sparingly soluble in alcohols.

3.2. X-ray crystallography

The crystal structure of $[Et_4N][Ta_6Br_{12}(H_2O)_6]Br_4 \cdot 4H_2O$ (**1**) consists of two different cations, $[Et_4N]^+$ and $[Ta_6Br_{12}(H_2O)_6]^{3+}$, Br^- anions and co-crystallized H_2O molecules. Both cations are located on the positions with four-fold inversion symmetry (4*a* and 4*b* *Wyckoff* sites). Therefore, the $[Ta_6Br_{12}(H_2O)_6]^{3+}$ cation consists of the symmetry independent atoms: Ta1, Ta2, O1, O2, Br1, Br2 and Br3 (Ta1 and O1 lie on the four-fold inversion axis). Similarly, in the $[Et_4N]^+$ cation, one ethyl moiety is symmetry independent [methylene carbon atoms C11 (first orientation) and C12 (second orientation) and methyl carbon atom C2], whereas nitrogen atom N1 lies on the four-fold inversion axis. The Br^- anions and co-crystallized H_2O molecules occupy general crystallographic positions of the $I4_1/a$ space group (16*f* *Wyckoff* sites); therefore, only one Br^- anion (Br4) and one of these H_2O molecules (O3) are symmetry independent. A thermal ellipsoid plot (at the 30% probability level) with the atomic numbering scheme consistent with the above described symmetry requirements is displayed in Fig. 1 (all symmetry codes used in the text, figures and tables are listed below the Table 3 as a footnote). Selected bond distances for **1** are given in Table 2.

The octahedral Ta_6 unit with an average Ta–Ta distance of 2.947 Å is surrounded by 12 bromido ligands capping all edges of the octahedron (with the Ta–Br distances of 2.587 Å on average). The Ta–Ta distances in **1** are somewhat smaller than the analogous distances in $[(Ta_6Br_{12})Br_3]$ (2.962 Å) [7a], but are larger than those in the structures with the diamagnetic $[Ta_6Br_{12}(H_2O)_6]^{2+}$ cluster cation (~2.898 Å) [2,3,17]. This elongation is consistent with a decrease in the number of electrons available for the metal–metal bonding (15 in $[Ta_6Br_{12}]^{3+}$ vs. 16 in $[Ta_6Br_{12}]^{2+}$) [6c,6d]. At the same time, the Ta–Br distances in the title compound are smaller than the analogous distances in the structures with $[Ta_6Br_{12}]^{2+}$ (~2.606 Å) [2,3,17]. Again, this contraction is consistent with the occupancy of the HOMO because it is known that this orbital possesses a metal–ligand antibonding character [6c,6d]. A larger number of electrons in this orbital enhance the metal–ligand antibonding interactions. The Ta_6 octahedron is slightly elongated in the direction of the four-fold inversion axis. The Ta–O bond distances (Table 2) are as usual for H_2O molecules occupying the L^a positions [2,3,17,18], although the bond lying in the direction of the four-fold inversion axis (Ta1–O1) is for 0.02 Å longer than the perpendicular one (Ta2–O2).

The C–N and C–C bond lengths in $[Et_4N]^+$ are as usually found for the corresponding type of single bonds [1.495 and 1.460 Å on average, respectively (taking into account both orientations of the cation)]. The two orientations of the $[Et_4N]^+$ cation can be brought

Table 2
Selected interatomic distances for **1** (Å).

Atoms	Distance	Atoms	Distance
Ta–Ta		*Ta–Br*	
Ta1–Ta2	2.947(1)	Ta1–Br1	2.586(1)
Ta1–Ta2^i	2.950(1)	Ta1–Br2	2.584(1)
Ta2–Ta2^i	2.944(1)	Ta2–Br1	2.591(1)
$\overline{d}$	2.947	Ta2–Br2^i	2.589(1)
		Ta2–Br3	2.585(1)
		Ta2–Br3^i	2.589(1)
		$\overline{d}$	2.587
Ta–O		*C–N*	
Ta1–O1	2.232(6)	N1–C11	1.49(1)
Ta2–O2	2.212(4)	N1–C12	1.50(2)
$\overline{d}$	2.222	$\overline{d}$	1.495
C–C			
C11–C2	1.50(1)		
C12–C2	1.42(3)		
$\overline{d}$	1.46		

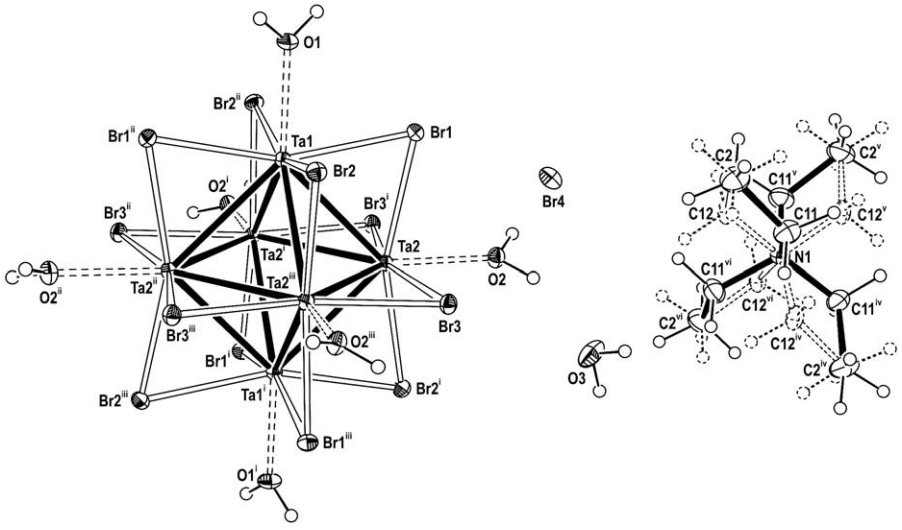

Fig. 1. The ORTEP plot of $[Et_4N][Ta_6Br_{12}(H_2O)_6]Br_4 \cdot 4H_2O$ **1** with the atomic numbering scheme (displacement ellipsoids are at 30% probability level).

almost into coincidence by an additional operation, i.e. by a two-fold rotation acting in the crystallographic direction [110]. Since the other parts of the structure are not affected by such an operation (for example, there is no mixing between Br^- anions and co-crystallized H_2O molecules), it is a non-crystallographic operation. Anyway, the conformation of the $[Et_4N]^+$ cation is identical in both orientations and is consistent with the S_4 molecular symmetry group. The same conformation and symmetry of this cation were observed also in the recently published structure of $[Et_4N]_2[K_2Nb_6Cl_{12}(CN)_6]$ [19]. Within the S_4 symmetry group, the $[Et_4N]^+$ cation has a prolate shape, with one spatial dimension larger than the other two. This becomes evident by looking at the distances between the particular pairs of methyl carbon atoms: the C2⋯C2^{v} distance is 3.53(1) Å, whereas the C2⋯C2^{iv} or C2⋯C2^{vi} distance is 4.45(1) Å (Fig. 1).

The title compound is an ionic solid and could be also described as a double salt $[Ta_6Br_{12}(H_2O)_6]Br_3 \cdot [Et_4N]Br \cdot 4H_2O$. Therefore, the largest part of its cohesive energy originates presumably from the electrostatic interactions between the charged constituents. Nevertheless, very often positions of hydrogen atoms enable hydrogen bonds to be created, which should contribute to the overall stability of a structure [in an ionic solid hydrogen bonds are usually related as "charge assisted hydrogen bonds" (CAHB) or "salt bridges" [20]]. The geometry parameters for the hydrogen bonds found in the crystal structure of the title compound are given in Table 3. As expected for CAHB, the acceptors are Br^- anions and O atoms from co-crystallized H_2O molecules.

Table 3
Hydrogen bonding geometry for **1** (Å, deg).

D–H⋯*A*	*D*–H	H⋯*A*	*D*⋯*A*	*D*–H⋯*A*
O1–H1⋯Br4^{vii}	0.83(4)	2.40(4)	3.231(4)	174(8)
O2–H21⋯O3	0.85(3)	1.83(5)	2.603(7)	151(6)
O2–H22⋯Br4	0.86(4)	2.36(4)	3.208(4)	175(8)
O3–H31⋯Br4^{iv}	0.85(5)	2.48(6)	3.307(6)	168(10)
O3–H32⋯Br4^{viii}	0.84(6)	2.59(7)	3.395(7)	161(6)

Symmetry codes used in the text, figures and tables: (i) 1/4–*y*, 1/4+*x*, 1/4–*z*; (ii) –*x*, 1/2–*y*, *z*; (iii) –1/4+*y*, 1/4–*x*, 1/4–*z*; (iv) 5/4–*y*, 1/4+*x*, 1/4–*z*; (v) 1–*x*, 3/2–*y*, *z*; (vi) –1/4+*y*, 5/4–*x*, 1/4–*z*; (vii) 3/4–*y*, 1/4+*x*, 1/4+*z*; (viii) –1/4+*y*, 3/4–*x*, –1/4+*z*; (ix) 1/2–*x*, 1/2–*y*, 1/2–*z*; (x) –1/2+*x*, *y*, 1/2–*z*; (xi) 1/4–*y*, –1/4+*x*, –1/4+*z*.

The set of hydrogen bonds connecting two neighbouring cluster cations could have a particular function in the expected intercluster magnetic exchange interactions (the clusters are paramagnetic centres) and deserves a special attention. The structural motif describing such a pair of neighbouring cluster units is shown in Fig. 2a. In the middle of the motif there is a centre of inversion, whereas around the line connecting cluster centres of gravity there are several Br^- anions and co-crystallized H_2O molecules. The cluster units are connected by six hydrogen-bonding bridges. Four of them are of the type: cation(I)⋯Br^-⋯H_2O(co-crystallized)⋯cation(II), and the two remaining bridges are of the type: cation(I)⋯Br^-⋯cation(II). All symmetry independent hydrogen bonds listed in Table 3 can be found in the motif shown in Fig. 2a. Structurally, all participating Br^- anions and co-crystallized H_2O molecules are rather far away from the central part of the motif, with the average distance from the centre of inversion being 5.9 Å. Even the coordinate H_2O molecules are relatively far away from this centre (~4.04 Å). On the contrary, the bridging ligands Br1, Br2 and Br3, and their symmetry equivalents Br1^{ix}, Br2^{ix} and Br3^{ix} (generated through the centre of inversion located in the middle of the motif) are close to each other; their distance from the centre of the motif is 2.6 Å on average. At the same time, the short intermolecular contacts Br1⋯Br2^{ix} [3.609(2) Å] and Br2⋯Br3^{ix} [3.626(2) Å] (Fig. 2a), point out to the places on the clusters where they touch other cluster units from the neighbourhood [the quoted contacts are shorter than the sum of the Van der Waals radii for two bromine atoms (3.7 Å)]. The above observation could be important for the analysis of possible intercluster magnetic exchange interactions. Namely, the theoretical calculations predict that the bridging ligand atoms participate in the formation of the HOMO [6d] and this orbital, occupied by only one electron, should be the natural magnetic orbital [21] of the $[Ta_6Br_{12}(H_2O)_6]^{3+}$ cluster unit.

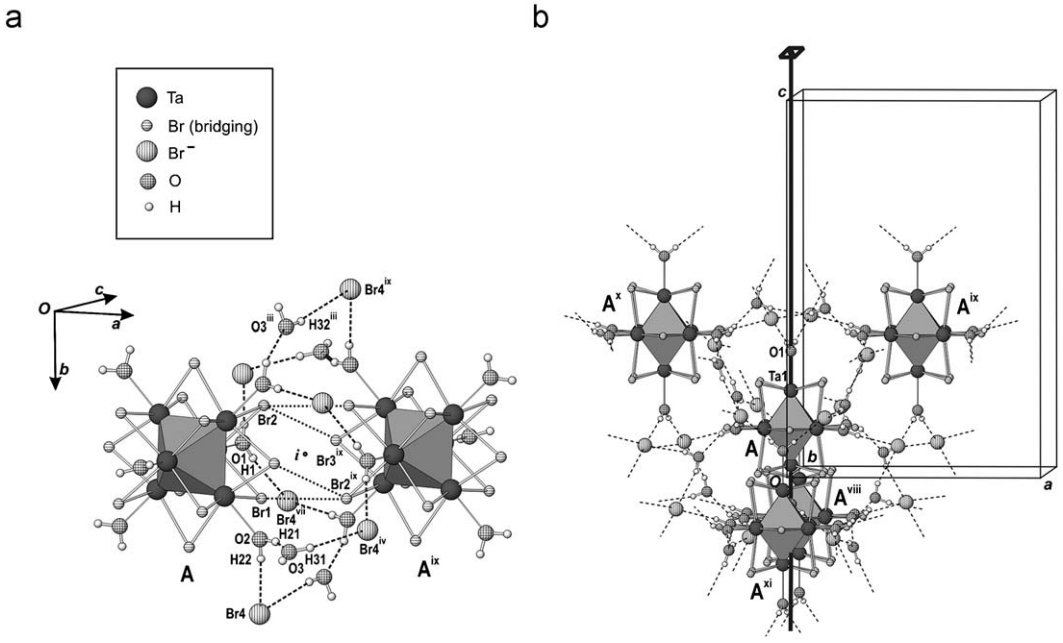

Fig. 2. Hydrogen bonds (dashed lines) inside one pair of the nearest neighbouring cluster units (a) and in the pattern formed by the central cluster unit and the four nearest neighbours (b). Symmetry independent hydrogen bonds from Table 3 and selected short intermolecular contacts (dotted lines) are labelled in (a). The hydrogen bond O3—H32⋯Br4^{viii} is represented by its symmetry equivalent O3^{iii}—H32^{iii}⋯Br4^{ix}.

As a consequence of the crystallographic four-fold inversion axes passing through the centres of cluster cations, the motif shown in Fig. 2a is repeated in four different directions in space (mutually non-collinear and non-coplanar). The hydrogen bonds existing between the two nearest neighbours are multiplied, and in the complete crystal structure, a complex three-dimensional hydrogen bonding network is formed (Fig. 2b). Another consequence of the four-fold inversion symmetry is a pattern of four nearest neighbouring cluster cations ($\mathbf{A}^{viii}$, $\mathbf{A}^{ix}$, $\mathbf{A}^{x}$ and $\mathbf{A}^{xi}$), that are all symmetry equivalent and with the same distance from the central **A** unit [8.906(3) Å]. This arrangement resembles the tetrahedral motif characteristic for the diamond lattice, although the present tetrahedron formed by the four nearest neighbours is not perfect [for example, the angle $\mathbf{A}^{ix}$–**A**–$\mathbf{A}^{x}$ is 106.8(1)°, the angle $\mathbf{A}^{viii}$–**A**–$\mathbf{A}^{x}$ is 110.8(1)°, Fig. 2b].

The similarity with the diamond lattice is not accidental, because the space group $I4_1/a$ is a subgroup of the diamond space group $Fd\bar{3}m$. In a group–subgroup chain [$Fd\bar{3}m$ (no. 227, origin choice 2)–$I4_1/a$ (no. 88, origin choice 2)], all *Wyckoff* sites can be correlated if the following transformation, between the (pseudo)-cubic coordinate system ($\boldsymbol{a}_c$, $\boldsymbol{b}_c$, $\boldsymbol{c}_c$) and the tetragonal coordinate system ($\boldsymbol{a}_t$, $\boldsymbol{b}_t$, $\boldsymbol{c}_t$) (Fig. 3) is used [22,23]:

$$\begin{pmatrix} \boldsymbol{a}_c \\ \boldsymbol{b}_c \\ \boldsymbol{c}_c \end{pmatrix} = \begin{pmatrix} 1 & 1 & 0 \\ -1 & 1 & 0 \\ 0 & 0 & 1 \end{pmatrix} \begin{pmatrix} \boldsymbol{a}_t \\ \boldsymbol{b}_t \\ \boldsymbol{c}_t \end{pmatrix} \quad (1)$$

In this way, the 4*a* and 4*b* *Wyckoff* sites of the tetragonal $I4_1/a$ space group (occupied by the $[Ta_6Br_{12}(H_2O)_6]^{3+}$ and $[Et_4N]^+$ cations, respectively) are transformed into the 8*a* and 8*b* *Wyckoff* sites of the cubic $Fd\bar{3}m$ space group [23]. Relation (1) and Fig. 3 show that the lengths of the $\boldsymbol{a}_c$ and $\boldsymbol{b}_c$ vectors are equal to the face diagonals of the square formed by the $\boldsymbol{a}_t$ and $\boldsymbol{b}_t$ vectors. In a perfect cubic symmetry this length should be equal to the length of the $\boldsymbol{c}_c$ vector. Using the unit cell parameter *a* [14.299(5) Å, Table 1] for the length of the $\boldsymbol{a}_t$ and $\boldsymbol{b}_t$ vectors and forcing the cubic symmetry, a value of 20.222(5) Å for the length of the $\boldsymbol{c}_c$ vector should be obtained ($\boldsymbol{c}_c = \sqrt{2}\boldsymbol{a}_t$). This value is for ~1 Å smaller than the value of the real unit cell parameter *c* [21.241(5) Å (Table 1)]. Thus, the high symmetry of the cubic group is destroyed and the original tetragonal symmetry appears to be a more accurate description of the crystal structure. The reason for the observed lengthening of the unit cell parameter *c* lies probably in the prolated shape of the $[Et_4N]^+$ cations which are aligned in the direction of the *c* axis. Moreover, a perfect cubic symmetry cannot be achieved if the $[Et_4N]^+$ cations occupy the 8*b* *Wyckoff* sites of the cubic $Fd\bar{3}m$ space group, because in that case, these cations should possess the tetrahedral T_d symmetry (T_d, i.e. $\bar{4}3m$ is the site symmetry of the 8*b* *Wyckoff* site of the space group $Fd\bar{3}m$). The $[Et_4N]^+$ cation, however, has no stable conformation within the T_d symmetry; therefore, the S_4 subgroup (i.e. $\bar{4}$ in the Hermann–Maugin notation) is a realistic site symmetry for the positions occupied by $[Et_4N]^+$. With a slightly longer unit cell parameter *c*, the resulting (pseudo)diamond lattice is somewhat distorted (elongated in the direction of the *c* axis). Consequently, the tetrahedral angles defined at the vertices of the lattice (occupied by cluster units) are not equal.

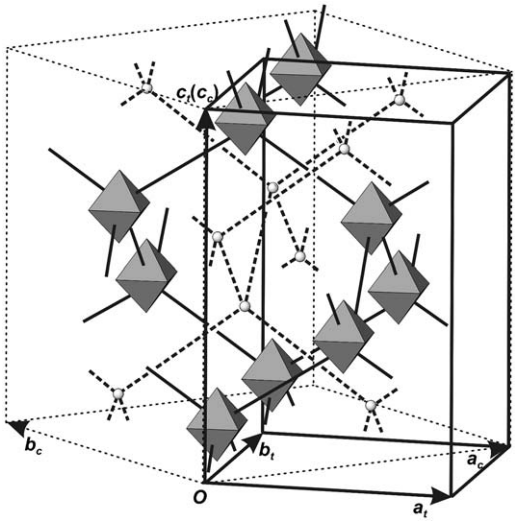

Fig. 3. Two interpenetrating (pseudo)diamond nets formed by the $[Ta_6Br_{12}(H_2O)_6]^{3+}$ units (shown as Ta_6 octahedra) and the $[Et_4N]^+$ cations (only N atoms are shown). One net is represented by solid lines, the other by dashed lines. The figure shows correspondence between the tetragonal ($\boldsymbol{a}_t$, $\boldsymbol{b}_t$, $\boldsymbol{c}_t$) and (pseudo)cubic ($\boldsymbol{a}_c$, $\boldsymbol{b}_c$, $\boldsymbol{c}_c$) unit cells.

The above given conclusions are in line with the structural properties of the cluster compound $[Me_4N][Ta_6Cl_{12}(H_2O)_6]Br_4$ (containing $[Me_4N]^+$ instead of $[Et_4N]^+$), the structure of which was solved and described in the $Fd\bar{3}m$ space group [7b]. The $[Me_4N]^+$ cation is smaller and possesses the T_d ($\bar{4}3m$) symmetry, so it can fit into the 8*b* (or 8*a*) *Wyckoff* sites of the space group $Fd\bar{3}m$. The $[Ta_6Cl_{12}(H_2O)_6]^{3+}$ cation (if we neglect hydrogen atoms of the coordinate water molecules) has an octahedral (O_h) symmetry, and can also fit into the 8*a* (or 8*b*) *Wyckoff* sites of the same space group. The resulting structural motif of $[Me_4N][Ta_6Cl_{12}(H_2O)_6]Br_4$ consists of two interpenetrating diamond nets of the NaTl type [24], with the positions of Br^- anions (disorderly occupied [7b]) located in between. The title compound shows a similar structural motif, but with the $[Ta_6Br_{12}(H_2O)_6]^{3+}$ and $[Et_4N]^+$ cations occupying 4*a* and 4*b* *Wyckoff* sites of the space group $I4_1/a$. The resulting motif is also a pair of interpenetrating (pseudo)diamond nets (Fig. 3, pseudo—because the nets are somewhat elongated in the direction of the *c* axis). The Br^- anions and co-crystallized H_2O molecules are located between the nets of the $[Ta_6Br_{12}(H_2O)_6]^{3+}$ and $[Et_4N]^+$ cations, and do not show any kind of disorder. The similarity between the structures of $[Me_4N][Ta_6Cl_{12}(H_2O)_6]Br_4$ and $[Et_4N][Ta_6Br_{12}(H_2O)_6]Br_4 \cdot 4H_2O$ is evident, but as they have to be described in two different space groups (connected through a group–subgroup relationship) this pair of structures can be considered as homeotypic [25].

Beside $[Me_4N][Ta_6Cl_{12}(H_2O)_6]Br_4$, several other compounds having the $[M_6X_{12}^i]^{n+}$ cluster core crystallize in the space group $Fd\bar{3}m$. In the structures of $[(Ta_6Cl_{12})Cl(H_2O)_5][HgBr_4] \cdot 9H_2O$ [7f] and $[(Ta_6Cl_{12})Cl(H_2O)_5][CdBr_4] \cdot 6H_2O$ [3] the paramagnetic $[(Ta_6Cl_{12})Cl(H_2O)_5]^{2+}$ [26] cluster units occupy one type of the tetrahedral sites (i.e. 8*a* *Wyckoff* sites), whereas the $[HgBr_4]^{2-}$ or $[CdBr_4]^{2-}$ anions occupy the other type of tetrahedral sites (i.e. 8*b* *Wyckoff* sites) inside their unit cells of the space group $Fd\bar{3}m$. The structure of $[(Ta_6Cl_{12})Cl(H_2O)_5][CdBr_4] \cdot 6H_2O$ is a particular one because for this compound intercluster magnetic exchange interactions were detected [3]. Among the cluster compounds with a diamagnetic cluster core there is a whole sequence of isostructural species all crystallizing in the $Fd\bar{3}m$ space group: $[Nb_6Cl_{12}(H_2O)_6][HgBr_4] \cdot 12H_2O$ [2] $[Ta_6Cl_{12}(H_2O)_6][HgBr_4] \cdot 12H_2O$ [2],$[Nb_6Cl_{12}(H_2O)_6][CdBr_4] \cdot 12H_2O$ [3] $[Ta_6Cl_{12}(H_2O)_6][CdBr_4] \cdot 12H_2O$ [3] and $[Ta_6Cl_{12}(H_2O)_6][ZnBr_4] \cdot 12H_2O$ [17]. Even the recently published structure of $(PyrH)_2[Nb_6Cl_{18}]$ was described in the $Fd\bar{3}m$ space group, where the diamagnetic cluster anions $[Nb_6Cl_{18}]^{2-}$ are located in the tetrahedral sites of the diamond lattice (i.e. 8*a* *Wyckoff* sites) [27]. Thus, a diamond-lattice structure with vertices occupied by the octahedral cluster units of the $[(M_6X_{12}^i)L_6^a]$ type seems to be a frequent structural motif in the solid state chemistry of niobium and tantalum halide cluster compounds.

3.3. Susceptibility measurements and EPR spectroscopy

The susceptibility measurements were performed by the Gouy method, at room temperature. For comparison, two compounds were recorded: the title compound (**1**) and the starting $Ta_6Br_{14}\cdot 8H_2O$ cluster. For **1** only a very small positive change of weight was found, giving the molar magnetic susceptibility $\chi_m = 8(2)\times 10^{-5}$ emu mol^{-1}. The measurement of $Ta_6Br_{14}\cdot 8H_2O$ showed somewhat larger, but negative change of weight with the susceptibility (χ_m) of $-32(2)\times 10^{-5}$ emu mol^{-1}, in accordance with the measurement done by Spreckelmeyer [28]. Molar magnetic susceptibility (χ_m) of cluster compounds are usually analyzed by means of the equation [1,2]:

$$\chi_m = \chi_{spin} + \chi^{dia}_{Pascal} + \chi^{dia}_{deloc} + \chi^{TIP} \quad (2)$$

where χ^{dia}_{Pascal} and χ^{dia}_{deloc} stand for diamagnetic contributions, whereas χ_{spin} and χ^{TIP} represent paramagnetic contributions. Using tabulated constants for particular constituents [1,29], the χ^{dia}_{Pascal} values are calculated as -89.8×10^{-5} and -69.2×10^{-5} emu mol^{-1}, for **1** and $Ta_6Br_{14}\cdot 8H_2O$, respectively. Diamagnetic χ^{dia}_{deloc} contributions originate from 15 or 16 electrons (Z) delocalized over the Ta_6 cluster units and they can be calculated using the formula $\chi^{dia}_{deloc} = -2.83\times 10^{10}\cdot Z\cdot \bar{r}^2$ ($\bar{r}$ = the mean radius of Ta_6 octahedra, 2.05×10^{-8} cm [1]). For the title compound (**1**), χ_{spin} should not be zero, because the compound contains paramagnetic cluster units with one unpaired electron, confirmed also by the EPR measurements (see below). Assuming the value of 54×10^{-5} emu mol^{-1} for χ^{TIP}[30], χ_{spin}, as calculated by Eq. (2), equals 62×10^{-5} emu mol^{-1}. This value is equivalent to the effective magnetic moment $\mu_{eff} = 1.2$ BM. This value is lower than expected for one unpaired electron (1.73 BM). However, such low values were also observed for Ta_6Br_{15} [1,4], Ta_6Cl_{15} [1,4] and $[(Ta_6Cl_{12})Cl_3(H_2O)_3]\cdot 3H_2O$ [1] (although at lower temperatures), where they indicated the intercluster magnetic exchange interactions. Temperature dependent magnetic susceptibility measurements, which should confirm such interactions in the title compound, are under investigation and will be presented in a separate paper.

The EPR spectrum of a powdered sample of **1**, recorded at room temperature, is shown in Fig. 4. The low intensity signal with $g\approx 3.93$ originates from the EPR cavity. The signal of compound **1** is a singlet, broad (peak-to-peak line-width $W\approx 50$ mT) approximate Lorentzian line with the effective g-value $g\approx 1.985$.

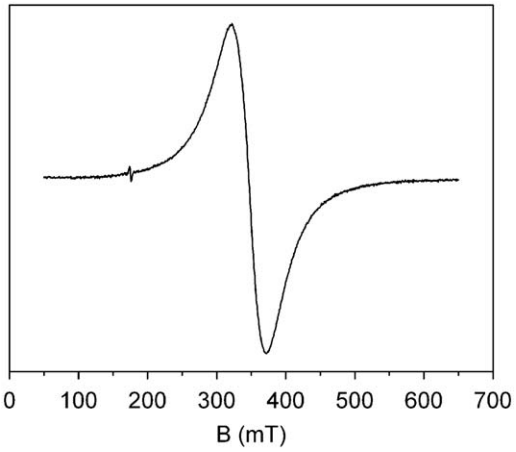

Fig. 4. X-band EPR spectrum of the powdered sample of $Ta_6Br_{14}\cdot 8H_2O$ at room temperature.

3.4. IR and UV/Vis spectroscopy

The infrared spectrum of **1** corroborates the presence of the two cations and water molecules. The absorption bands at 3475–3400 and 3200 cm^{-1}, with those at 1620 and 1608 cm^{-1}, correspond to ν(O–H) and δ(H–O–H) of the co-crystallized and coordinate water molecules [31]. The bands arising between 3050 and 2850 cm^{-1} originate from $\nu(CH_2)$ and $\nu(CH_3)$ of the organic cation, whereas the accompanying deformation modes give rise to the bands in the 1470–1370 cm^{-1} region. Other bands from Et_4N^+ relate to the CH_2 twisting (1303 cm^{-1}), CH_3 and CH_2 rocking (1182 and 1004, and 792 cm^{-1}, respectively), and the C–C and C–N stretching (1078 and 1032 cm^{-1}, respectively) vibrations [32]. Also of significant intensities are the absorption bands found in the 570–450 cm^{-1} region, where different (rocking, twisting and waging) modes of coordinate water molecules appear, as well as the Ta–O(H_2O) stretching vibrations [31]. In the far infrared region of the spectrum of **1**, several absorption bands appear. The strongest (split) band, with two resolved maxima at 230 and 226 cm^{-1}, can be attributed to the Ta–Br^i (i = inner, bridging ligand) stretching vibration [33,34]. The corresponding band in the spectra of the starting $Ta_6Br_{14}\cdot 8H_2O$ cluster and of other compounds containing $[Ta_6Br_{12}]^{2+}$ was found at the same region (230–224 cm^{-1}) [33,35,36]. Since all terminal positions of the octahedral cluster unit in **1** are occupied by H_2O molecules (L^a positions), the ν(Ta–Br^a) absorption band, as the one more sensitive to the oxidation state of the cluster, could not be present in the spectrum of the title compound. Therefore, the FIR spectra cannot help in assigning the oxidation state of the cluster core in **1**, although they proved to be a very useful test for predicting the oxidation state for a series of compounds with $[M_6Cl_{12}]^{n+}$ [37].

The solid-state electronic spectrum of **1**, together with the spectrum of the starting $Ta_6Br_{14}\cdot 8H_2O$ cluster, containing $[Ta_6Br_{12}]^{2+}$, is shown in Fig. 5. Three absorption bands observed in the visible region of the spectrum of **1**, with the maxima at 762, 868 and 963 nm, strongly substantiate a paramagnetic cluster compound with the $[Ta_6Br_{12}]^{3+}$ cluster core [38–40]. The absence of any absorption in the region between 600 and 700 nm, where the $[Ta_6Br_{12}]^{2+}$ cluster unit absorbs (Fig. 5), clearly demonstrates that a complete transformation of the cluster from the oxidation state 2+ into the oxidation state 3+ took place.

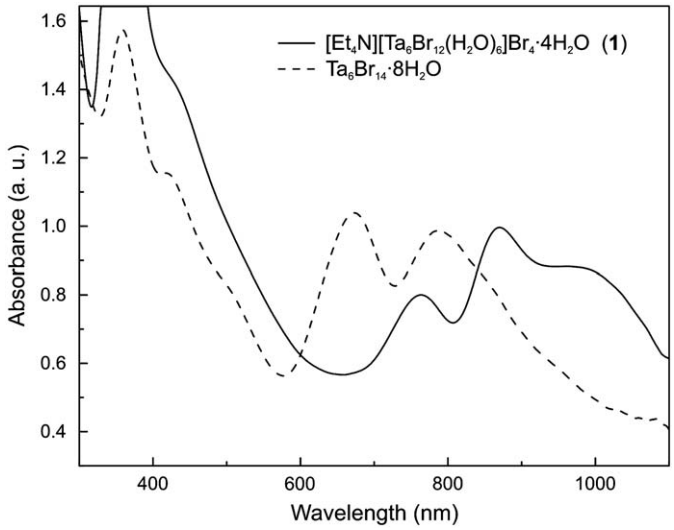

Fig. 5. The solid-state electronic spectra of the title compound **1** (solid line) and of the starting $Ta_6Br_{14}\cdot 8H_2O$ cluster (dashed line).

3.5. Thermal study

The thermal properties of the title compound were followed by a simultaneous TG/DTA analysis. On heating, the compound was stable up to 75 °C, when its thermal decomposition began by elimination of water molecules. All water molecules are lost in one step, between 75 and 135 °C, with a mass loss of 6.71% (calc. 6.74% for 10 H_2O) by an endothermic process (the accompaning DTA maximum at 121 °C). It appears that the CAHB hydrogen bonding network connects the co-crystallized water molecules as tightly as the coordinative bonds holding (coordinate) water molecules bound to Ta atoms, because the expected splitting of the above described TG step was not observed. During the further decomposition process, the majority of the mass of the sample was being lost between 135 and 400 °C, exothermally, but without properly resolved steps in the TG curve. The constant mass rest after 700 °C corresponded to Ta_2O_5 (found 48.74%, calc. 49.57%).

4. Conclusions

The new cluster $[Et_4N][Ta_6Br_{12}(H_2O)_6]Br_4 \cdot 4H_2O$ **1** formed as a reaction product of the air-oxygen oxidation of diamagnetic $[Ta_6Br_{12}]^{2+}$ to paramagnetic $[Ta_6Br_{12}]^{3+}$ in the presence of Et_4NBr. The cluster crystallizes in the tetragonal $I4_1/a$ space group with a crystal structure arrangement that is similar to that one found for a number of other cluster-related compounds crystallizing in the diamond $Fd\bar{3}m$ cubic space group. The data indicate that the specific conformation of the $[Et_4N]^+$ cation is responsible for the lengthening of the unit cell parameter c and for the reduction of the high symmetry of the cubic $Fd\bar{3}m$ group into the symmetry of the tetragonal $I4_1/a$ group. Nevertheless, the important four-fold inversion crystallographic symmetry is retained, giving rise to the emanation of the three-dimensional (pseudo)diamond lattice of the paramagnetic $[Ta_6Br_{12}(H_2O)_6]^{3+}$ cluster entities. A detailed structural analysis shows that the nearest neighbouring cluster units create short intermolecular contacts across the bridging bromine atoms.

Supplementary data

Crystallographic data (excluding structure factors) for the structure reported in this paper have been deposited with the Cambridge Crystallographic Data Centre as supplementary publication no. CCDC 721268. Copies of the data can be obtained free of charge on application to CCDC, 12 Union Road, Cambridge CB2 1EZ, UK (fax: +44 1223 336-033; e-mail: deposit@ccdc.cam.ac.uk).

Acknowledgments

This research was supported by the Ministry of Science, Education and Sports of the Republic of Croatia (Grant no. 098-0982904-2946). The authors are also grateful to Dr. Dijana Žilić from Ruđer Bošković Institute for recording the EPR spectrum of the title compound.

Appendix A. Supplementary material

Supplementary data associated with this article can be found in the online version at doi:10.1016/j.jssc.2009.06.026.

References

[1] J.G. Converse, R.E. McCarley, Inorg. Chem. 9 (1970) 1361–1366.
[2] M. Vojnović, S. Antolić, B. Kojić-Prodić, N. Brničević, M. Miljak, I. Aviani, Z. Anorg. Allg. Chem. 623 (1997) 1247–1254.
[3] M. Vojnović, N. Brničević, I. Bašic, R. Trojko, M. Miljak, I.D. Desnica-Franković, Mater. Res. Bull. 36 (2001) 211–225.
[4] D. Bauer, H.-G. von Schnering, Z. Anorg. Allg. Chem. 361 (1968) 259–276.
[5] R. Knoll, J. Sokolowski, Y. Benhaim, A.I. Shames, S.D. Goren, H. Shaked, J.-Y. Thépot, C. Perrin, S. Cordier, Physica B 381 (2006) 47–52.
[6] [a] F.A. Cotton, T.E. Haas, Inorg. Chem. 3 (1964) 10–17;
[b] D.J. Robbins, A.J. Thomson, J. Chem. Soc. Dalton Trans. (1972) 2350–2364;
[c] T. Hughbanks, Prog. Solid State Chem. 19 (1989) 329–372;
[d] F. Ogliaro, S. Cordier, J.-F. Halet, C. Perrin, J.-Y. Saillard, M. Sergent, Inorg. Chem. 37 (1998) 6199–6207.
[7] [a] H.-G. von Schnering, D. Vu, S.-L. Jin, K. Peters, Z. Kristallogr. NCS 214 (1999) 15;
[b] N. Brničević, Ž. Ružić-Toroš, B. Kojić-Prodić, J. Chem. Soc., Dalton Trans. (1985) 455–458;
[c] H. Imoto, S. Hayakawa, N. Morita, T. Saito, Inorg. Chem. 29 (1990) 2007–2014;
[d] N. Brničević, D. Nöthig-Hus, B. Kojić-Prodić, Ž. Ružić-Toroš, Ž. Danilović, R.E. McCarley, Inorg. Chem. 31 (1992) 3924–3928;
[e] N. Prokopuk, V.O. Kennedy, C.L. Stern, D.F. Shriver, Inorg. Chem. 37 (1998) 5001–5006;
[f] N. Brničević, M. Vojnović, S. Antolić, B. Kojić-Prodić, I.D. Desnica-Franković, Solid State Sci. 1 (1999) 483–495;
[g] S. Cordier, C. Loisel, C. Perrin, M. Sergent, J. Solid State Chem. 147 (1999) 350–357;
[h] M. Vojnović, D. Jozić, I. Bašic, S. Rončević, P. Planinić, Acta Crystallogr. C 60 (2004) m33–m34;
[i] P. Planinić, V. Rastija, B. Perić, G. Giester, N. Brničević, C.R. Chimie 8 (2005) 1766–1773;
[j] F.W. Koknat, R.E. McCarley, Inorg. Chem. 13 (1974) 295–300;
[k] A. Pénicaud, P. Batail, C. Perrin, C. Coulon, S.S.P. Parkin, J.B. Torrance, J. Chem. Soc. Chem. Commun. (1987) 330–332;
[l] S. Ihmaïne, C. Perrin, O. Peña, M. Sergent, J. Less-Common Met. 137 (1988) 323–332;
[m] A. Pénicaud, P. Batail, P. Davidson, A.-M. Levulet, C. Coulon, C. Perrin, Chem. Mater. 2 (1990) 117–123;
[n] L. LePolles, S. Cordier, C. Perrin, M. Sergent, C.R. Acad. Sci. II C 2 (1999) 661–667;
[o] N. Prokopuk, C.S. Weinert, V.O. Kennedy, D.P. Siska, H.–J. Jeon, C.L. Stern, D.F. Shriver, Inorg. Chim. Acta 300 (2000) 951–957;
[p] S. Cordier, O. Hernandez, C. Perrin, J. Solid State Chem. 158 (2001) 327–333;
[q] S. Cordier, O. Hernandez, C. Perrin, J. Solid State Chem. 163 (2002) 319–324;
[r] A. Flemming, M. Köckerling, Z. Anorg. Allg. Chem. 634 (2008) 2309–2315.
[8] O. Peña, S. Ihmaïne, C. Perrin, M. Sergent, Solid State Commun. 74 (1990) 285–290.
[9] S. Cordier, C. Perrin, M. Sergent, J. Solid State Chem. 118 (1995) 274–279.
[10] F.W. Koknat, J.A. Parsons, A. Vangvusharintra, Inorg. Chem. 13 (1974) 1699–1702.
[11] A. Kashta, N. Brničević, R.E. McCarley, Polyhedron 10 (1991) 2031–2036.
[12] H. Schäfer, K.-D. Dohmann, Z. Anorg. Allg. Chem. 300 (1959) 1–32.
[13] Z. Otwinowski, W. Minor, in: C.W. Carter, R.M. Sweet (Eds.), Methods in Enzymology, Macromolecular Crystallography, Part A, vol. 276, Academic Press, London, 1997, p. 307.
[14] KappaCCD User Manual, revision 1.10, Bruker Nonius BV, Delft, The Netherlands, 1998.
[15] A. Altomare, G. Cascarano, C. Giacovazzo, A. Gualardi, J. Appl. Crystallogr. 26 (1993) 343–350.
[16] G.M. Sheldrick, SHELXL-97, Program for Crystal Structure Refinement, 1997.
[17] M. Vojnović, I. Bašic, N. Brničević, Z. Kristallogr. NCS 214 (1999) 435.
[18] M. Vojnović, N. Brničević, I. Bašic, P. Planinić, G. Giester, Z. Anorg. Allg. Chem. 628 (2002) 401–408.
[19] J.-J. Zhang, J. Glaser, S.A. Gamboa, A. Lachgar, J. Chem. Crystallogr. 39 (2009) 1–8.
[20] C. Giacovazzo, Fundamentals of Crystallography, Oxford University Press, Oxford, 2002.
[21] O. Kahn, Molecular Magnetism, Wiley, New York, 1993.
[22] E. Kroumova, J.M. Perez-Mato, M.I. Aroyo, J. Appl. Crystallogr. 31 (1998) 646.
[23] 〈http://www.cryst.ehu.es/cryst/wpsplit.html〉.
[24] M. O'Keeffe, M. Eddaoudi, H.L. Li, T. Reineke, O.M. Yaghi, J. Solid State Chem. 152 (2000) 3–20.
[25] J. Lima-De-Faria, E. Hellner, F. Liebau, E. Makovicky, E. Parthé, Acta Crystallogr. A 46 (1990) 1–11.
[26] In the $[(Ta_6Cl_{12})Cl(H_2O)_5]^{2+}$ unit there is a $[Ta_6Cl_{12}]^{3+}$ cluster core, because one Cl^- anion and 5 H_2O molecules disorderly occupy six terminal positions L^a.
[27] A. Flemming, A. Hoppe, M. Köckerling, J. Solid State Chem. 181 (2008) 2660–2665.
[28] B. Spreckelmeyer, Z. Anorg. Allg. Chem. 358 (1968) 147–162.
[29] P.W. Selwood, Magnetochemistry, second ed., Interscience, New York, 1956.

[30] From Ref. [1] $\chi^{TIP}[Ta_6Cl_{12}]^{4+} \approx 501 \times 10^{-6}$ emu mol^{-1}, whereas $\chi^{TIP}[Ta_6Cl_{12}]^{3+} \approx 497 \times 10^{-6}$ emu mol^{-1}. From the same reference $\chi^{TIP}[Ta_6Br_{12}]^{4+} \approx 544 \times 10^{-6}$ emu mol^{-1}. From these data we estimated $\chi^{TIP}[Ta_6Br_{12}]^{3+}$ to be 540×10^{-6} emu mol^{-1}.
[31] K. Nakamoto, Infrared and Raman Spectra of Inorganic and Coordination Compounds, fifth ed., Wiley, New York, 1997.
[32] W.H.J. de Beer, A.M. Heyns, Spectrochim. Acta 37A (1981) 1099–1107.
[33] R. Mattes, Z. Anorg. Allg. Chem. 364 (1969) 279–289.
[34] P.B. Fleming, J.L. Meyer, W.K. Grindstaff, R.E. McCarley, Inorg. Chem. 9 (1970) 1769–1771.
[35] N. Brničević, Z. Anorg. Allg. Chem. 441 (1978) 230–236.
[36] K. Harder, W. Preetz, Z. Anorg. Allg. Chem. 591 (1990) 32–40.
[37] P. Caillet, S. Ihmaine, C. Perrin, J. Mol. Struct. 216 (1990) 27–40.
[38] B. Spreckelmeyer, Z. Anorg. Allg. Chem. 365 (1969) 225–338.
[39] P.B. Fleming, R.E. McCarley, Inorg. Chem. 9 (1970) 1347–1354.
[40] C.L. Hussey, R. Quigley, K.R. Seddon, Inorg. Chem. 34 (1995) 370–377.